



Thermal resistance effect on anomalous diffusion of molecules under confinement

Jiamin Yuan^{a,b}, Zhiqiang Liu^{a,1}, Yimo Wu^{b,c}, Jingfeng Han^c, Xiaomin Tang^{a,b}, Chengbin Li^a, Wei Chen^a, Xianfeng Yi^a, Jian Zhou^d, Rajamani Krishna^e, German Sastre^f, and Anmin Zheng^{a,1}

^aState Key Laboratory of Magnetic Resonance and Atomic and Molecular Physics, National Center for Magnetic Resonance in Wuhan, Key Laboratory of Magnetic Resonance in Biological Systems, Wuhan Institute of Physics and Mathematics, Innovation Academy for Precision Measurement Science and Technology, Chinese Academy of Sciences, 430071 Wuhan, China; ^bUniversity of Chinese Academy of Sciences, 100049 Beijing, China; ^cNational Engineering Laboratory for Methanol to Olefins, State Energy Low Carbon Catalysis and Engineering R&D Center, Dalian National Laboratory for Clean Energy, iChEM (Collaborative Innovation Center of Chemistry for Energy Materials), Dalian Institute of Chemical Physics, Chinese Academy of Sciences, 116023 Dalian, Liaoning, China; ^dShanghai Research Institute of Petrochemical Technology, Sinopec, 201208 Shanghai, China; ^eVan't Hoff Institute for Molecular Sciences, University of Amsterdam, 1098 XH Amsterdam, The Netherlands; and ^fInstituto de Tecnología Química, Consejo Superior de Investigaciones Científicas, Universitat Politècnica de Valencia, 46022 Valencia, Spain

Edited by Alexis T. Bell, University of California, Berkeley, CA, and approved April 6, 2021 (received for review February 2, 2021)

Diffusion is generally faster at higher temperatures. Here, a counterintuitive behavior is observed in that the movement of long-chain molecules slows as the temperature increases under confinement. This report confirms that this anomalous diffusion is caused by the “thermal resistance effect,” in which the diffusion resistance of linear-chain molecules is equivalent to that with branched-chain configurations at high temperature. It then restrains the molecular transportation in the nanoscale channels, as further confirmed by zero length column experiments. This work enriches our understanding of the anomalous diffusion family and provides fundamental insights into the mechanism inside confined systems.

zeolite | molecular dynamics | anomalous diffusion | confinement | thermal resistance effect

Molecules or atoms are subject to permanent random movement as a consequence of their thermal energy in the condensed phase (i.e., Brownian motion). The diffusion process is a universal phenomenon that occurs on different time scales in all states of matter (1). It is critically important in the separation and catalytic processes involving the application of nanoporous materials (2–5).

Besides the condensed phase, diffusion in the confined space of channels at nanoscale (i.e., less than 1 nm) has spurred significant interest recently (5). Of the various nanoporous materials, zeolites with regular crystalline shapes and a wide variety of topologies are well known due to their widespread use in industrial applications but also their widespread study on the microscale (3). An intriguing case of molecular movement inside a zeolite is called “single-file diffusion”; this only occurs in one-dimensional (1-D) channels where the molecules cannot pass each other, and a dramatic increase in mobility of the molecules could be observed (6). Single-file diffusion has been found in many materials with 1-D channels; this has been detected by NMR experiments (7–9). Derouane and coworkers found the “levitation effect” for the maximum self-diffusivity of a molecule whose diameter is close to the pore size of zeolite (10). Nag et al. illustrated the efficacy of the levitation effect for separating mixtures of both linear n-pentane and its branched isomer (11). Other interesting effects include incommensurate diffusion (12, 13), molecular traffic control (14), resonance diffusion (15, 16), window effect (17), and molecular path control (18). Anomalous diffusion is still being discovered and continues to be an exciting field of research with many surprises.

For all the diffusion behavior (i.e., normal and anomalous described above), the transport of sorbate is influenced by temperature. Generally, the diffusivity and temperature follow the Arrhenius equation (Eq. 1). Thus, a higher temperature leads to faster diffusion behavior (19, 20):

$$D_s = D_0 e^{-\frac{E_a}{RT}} \quad [1]$$

Here, D_s represents the self-diffusion coefficient, D_0 is a pre-exponential factor, E_a stands for the diffusion activation energy,

and R and T are the molar gas constant and temperature, respectively. For instance, Ghysels et al. showed that the diffusion coefficients (D_s) of ethene in several zeolites have a monotonic increase with temperature (21). Gao et al. measured the diffusion coefficients of different alkane species at different temperatures in various zeolites by pulsed field gradient NMR (PFG-NMR) and found that they follow Eq. 1 as well. In this work, an anomalous effect for long-chain molecules (i.e., alkane and alkene [SI Appendix, Table S2]) inside MFI zeolite (silicalite-1) was observed, where the diffusion coefficient slowed with increasing temperature for n-dodecane (C12) molecules (Fig. 1B). Although the diffusion of C12 has been investigated in zeolites, this phenomenon had not been reported yet (16, 22–26). The connection between the structure and anomalous diffusion has been established based on molecular dynamics (MD) simulations and zero length column (ZLC) experiments, which provide fundamental insights into the diffusion properties inside confined channels.

Results

The diffusion behaviors of molecules inside the confined channel are strongly correlated with the framework of the zeolite. Fig. 1A

Significance

Diffusion is the primary process in practical multidisciplinary areas such as separation and catalysis. Transportation is usually positively correlated with temperature due to thermal motion. We show here an anomalous phenomenon wherein a higher temperature effectively slows diffusion for linear-chain hydrocarbon molecules under confinement. Such an obstruction in diffusion results from the novel mechanism of “thermal resistance effect,” in which the configuration of a guest molecule is significantly deformed with temperature effect and then strongly restrains the process of transportation in nanoscale channels at high temperature. This work will enrich our understanding of an anomalous mechanism of the diffusion phenomenon and could shed light on a fundamental understanding of the diffusion process.

Author contributions: A.Z. designed research; J.Y., Z.L., Y.W., and J.H. performed research; J.Y., Z.L., X.T., C.L., W.C., X.Y., J.Z., R.K., and G.S. analyzed data; and Z.L. and A.Z. wrote the paper.

The authors declare no competing interest.

This article is a PNAS Direct Submission.

Published under the PNAS license.

¹To whom correspondence may be addressed. Email: zqliu@wipm.ac.cn or zhenganm@wipm.ac.cn.

This article contains supporting information online at <https://www.pnas.org/lookup/suppl/doi:10.1073/pnas.2102097118/-DCSupplemental>.

Published May 17, 2021.

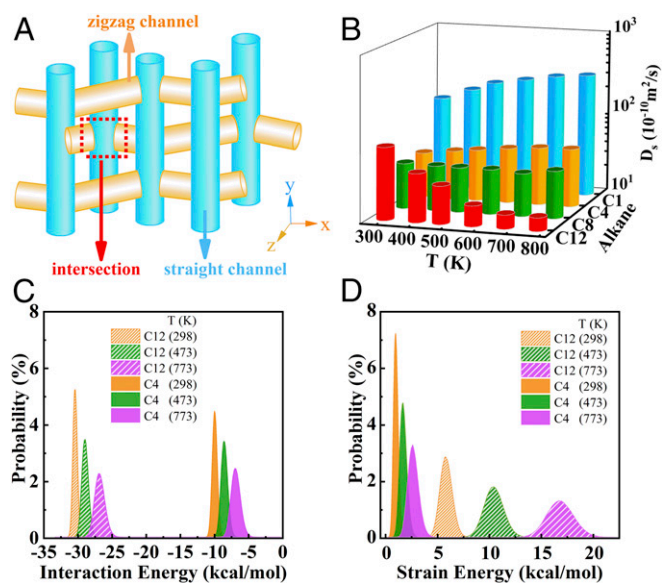


Fig. 1. (A) Three-dimensional channels of MFI zeolite. The blue and orange cylinders represent the straight and zigzag channels, respectively. (B) Self-diffusion coefficients of methane (C1), *n*-butane (C4), *n*-octane (C8), and *n*-dodecane (C12) in MFI zeolite at different temperatures. (C) Distributions of interaction energy between molecules and MFI zeolite, and (D) distributions of strain energy for alkane molecules (*n*-butane [C4] and *n*-dodecane [C12]) at 298, 473, and 773 K.

shows the three-dimensional (3-D) channels of MFI, which possess 10-ring zigzag channels with a window size of $5.1 \text{ \AA} \times 5.5 \text{ \AA}$ along the X and Z direction, as well as 10-ring straight channel ($5.3 \text{ \AA} \times 5.6 \text{ \AA}$) distributed in the Y direction (SI Appendix, Fig. S1A). It is well known that the self-diffusion coefficient (D_s) could quantitatively describe the movement of guest molecules inside confined channels (22). In this work, the D_s of linear alkane molecules (i.e., methane [C1], *n*-butane [C4], *n*-octane [C8], and *n*-dodecane [C12]) were studied because they are the main components of natural gas, gasoline, and diesel and are widely investigated in the petrochemical industry (23). The results show that D_s of alkane inside MFI agrees with Jobic's work on the order from 10^{-9} to $10^{-8} \text{ m}^2/\text{s}$ (24, 25). SI Appendix, Table S1 shows that the simulated D_s of methane at 473 K is $\sim 2.21 \times 10^{-8} \text{ m}^2/\text{s}$, which is almost the same as experimental result ($2.05 \times 10^{-8} \text{ m}^2/\text{s}$) detected by quasi-elastic neutron scattering (QENS) at the same temperature (24). As for C4 at ambient temperature, our result ($0.35 \times 10^{-8} \text{ m}^2/\text{s}$) is also on the same order of Leroy and coworkers ($0.41 \times 10^{-8} \text{ m}^2/\text{s}$) (26). In addition, Runnebaum and coworkers reported D_s of C12 in zeolite MFI at 400 K ($\sim 0.40 \times 10^{-8} \text{ m}^2/\text{s}$) (16). Thus, further confirming the validity of our calculations ($0.39 \times 10^{-8} \text{ m}^2/\text{s}$).

According to Eq. 1, the D_s of linear alkane molecules is strongly dependent on the temperature. Fig. 1B shows that for the short-chain alkane molecules (i.e., C1 and C4), the diffusion is positively correlated with temperature, because the higher temperature increased the thermal movement. However, in contrast to short-chain alkanes, there is no monotonic increase of D_s as temperature increases for long-chain paraffin (e.g., C8 and C12). In particular for C12, a counterintuitive diffusion behavior was determined whereby the movement of molecules slowed down as the temperature increases. D_s is $0.76 \times 10^{-8} \text{ m}^2/\text{s}$ at 298 K, but it inversely decreases to 0.29×10^{-8} and $0.15 \times 10^{-8} \text{ m}^2/\text{s}$ at 473 K and 773 K, respectively (SI Appendix, Table S1). Apparently, an anomalous diffusion as a function of temperature variations inside zeolite was observed.

Diffusion behaviors are closely related to the interaction between adsorbate and zeolite framework (20). Thus, the interaction energy and strain energy (configuration energy) of C4 and C12 were investigated to understand the anomalous diffusion. Fig. 1C shows that the interaction energy within zeolite for C12 is approximately threefold stronger than that for C4 due to its longer chain. However, there was no notable variance on this quantity for both C4 and C12 at different temperatures, which indicates that the interaction energy may not be the main factor that induces the anomalous diffusion. However, the strain energy is within 5 kcal/mol with the variation of temperature for C4. The strain energy is significantly increased from 6 kcal/mol (298 K) to 17 kcal/mol (773 K) for C12 (Fig. 1D). The larger strain energy clearly indicated the severe structural distortion for C12 at a relatively high temperature.

The structural distortion was also quantitatively confirmed by the intramolecular bending angle of the molecule. Fig. 2A and SI Appendix, Figs. S2 and S3A show that the number (ratio) of bending molecules increases with increasing temperature: 40% of C12 with the intramolecular C-C-C angle are distorted by more than 45° at 298 K (Fig. 2A), while almost 90% are larger than 45° under 773 K, which confirmed its pronounced deformation. Thus, the anomalous diffusion may be caused by the structural deformation of the long-chain paraffin.

To further determine the effect of the molecular deformation with the increasing temperature on the anomalous diffusion in MFI zeolite, we performed a theoretical simulation on the basis of a model, which only contains fixed structure without any structural deformation (as rigid molecule) for C4 and C12. As shown in Fig. 2B, structural distortion contributes to diffusion deceleration for short chain alkanes like C4. For instance, the D_s of C4 are 0.43×10^{-8} , 0.61×10^{-8} , and $0.81 \times 10^{-8} \text{ m}^2/\text{s}$ at 298, 473, and 773 K, respectively, which are slightly larger than the according flexible model (i.e., 0.35×10^{-8} [298 K], 0.42×10^{-8} [473 K], and 0.51×10^{-8} [773 K] m^2/s). The molecular bending inside the zeolite confined space could hinder the mass transfer even for the short chain C4 but still maintain a positive correlation for the significant contribution of the kinetic energy for high temperature. In contrast to C4, the D_s of C12 with rigid and

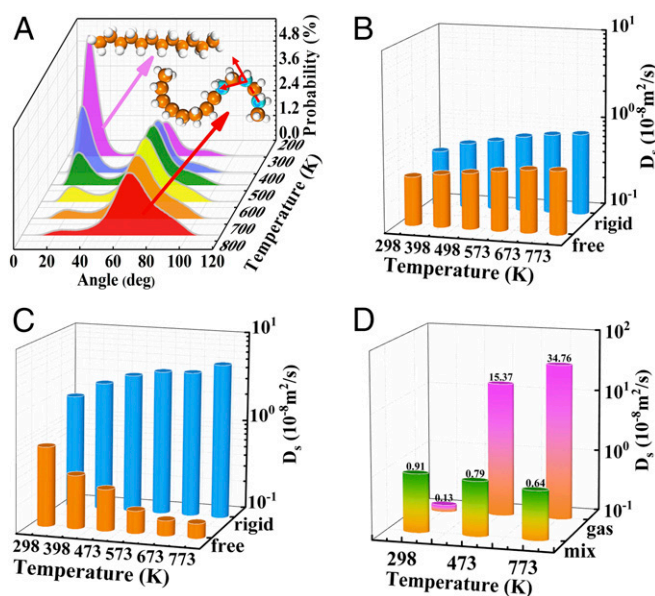


Fig. 2. (A) Distributions of distorted angle for *n*-dodecane at various temperatures. (B) D_s of rigid C4 (linear-C4, blue histogram), and free C4 (flexible C4, orange histogram). (C) D_s of rigid C12 (linear-C12, blue histogram) and free C12 (flexible C12, orange histogram). (D) D_s of mixture for rigid linear-C12/branched-C12 (green orange gradient histogram) inside MFI and at gas phase (pink orange gradient histogram) at 298, 473, and 773 K.

flexible construction possessed an antipodal temperature dependence. Fig. 2C clearly indicates that the anomalous diffusion disappeared and presented a positive relationship between D_s and the temperature when the rigid C12 is applied. For example, the self-diffusion coefficients of rigid C12 molecules are 1.83×10^{-8} (298 K), 3.45×10^{-8} (473 K), and 5.18×10^{-8} m²/s (773 K). In addition, a controllable simulation of a mixture of rigid linear C12 and rigid branched C12 both without deformation was applied to check the effect of concentration of branched-chain component (i.e., $M_{n-C12}/M_{branched-C12}$) on the diffusion properties. According to MD simulation, the relative ratios of $M_{linear-C12}/M_{branched-C12}$ were varied with temperature (e.g., 8:4, 4:8, 2:10 at 298 K, 473 K, and 773 K). Interestingly, the diffusion coefficients are indeed reduced as the temperature increased (Fig. 2D), which agrees with the trend of realistic simulation for flexible n-dodecane (C12) in MFI zeolite (Fig. 1B), suggesting that the significant diffusion resistance of linear-chain molecules is due to the presence of branched-chain-like configurations at high temperatures.

Quantitative comparison of molecular deformation at different temperatures will further illustrate the anomalous effect. The root-mean-square deviation (RMSD) of Cartesian positions is a standard parameter to evaluate the molecular deformation in the confined zeolite (SI Appendix, Table S3) (27). The value of RMSD is calculated by comparing the minimum position changes of the reference configuration and the transient one. The RMSD of C4 is less than 1.0 Å even at 773 K (Fig. 3A), and the two peaks at 0.5 and 1 Å are the smaller and the larger distortion of the adsorbates consistent with the results mentioned above; the molecular deformation increases gradually as the temperature increases. The peak at 1 Å enhances while the peak at 0.5 Å reduces. This is why the strain energy increases as the temperature goes up. In C12, a peak at 2.0 Å was observed at 773 K (Fig. 3A), which means that the long chain molecule is dramatically distorted at higher

temperatures. Furthermore, a wide distribution of RMSD of C12 with high temperatures is apparently illustrated such that the linear structure of C12 at low temperatures was gradually undermined, and a more notable deformation was present at higher temperatures. This consequently led to the anomalous diffusion.

The width (the second largest size) of the molecule inside the confined space has a great impact on the diffusion process (refer to SI Appendix for the specific calculation method). Fig. 3B illustrates that a higher temperature leads to a larger value of C12's molecule width as well as slows the diffusion. For example, the width is distributed in 4.6 Å at 298 K, but it increased to 4.8 Å and 5.4 Å at 473 K and 773 K, respectively. One is more likely to find a larger molecule with slow movement under higher temperatures. As mentioned above, molecules get shorter (length) (SI Appendix, Fig. S4) and broader (width and height) (Fig. 3B and SI Appendix, Fig. S5) in shape because the higher temperature causes molecular bending. Therefore, the diffusion was strongly hindered at high temperatures for a larger C12. There was also negative correlation between diffusion coefficient and temperature (The length and height of C12 are plotted in SI Appendix, Fig. S5).

A thermistor is a temperature sensitive component, and the thermistor with a positive temperature coefficient has a larger resistance under the higher temperature (28). Interestingly, this anomalous behavior shows a similar property to thermistors and thus can be named as the "thermal resistance effect" (TRE) in the diffusion process. The temperature could lead to a decreased diffusion coefficient of C12 due to the structural distortion of long-chain alkanes (Figs. 2A and 4). Furthermore, bending molecules not only blocks the diffusion of the induced-bulky configuration themselves but also strongly obstruct the movement of the other linear component during the diffusion process (as shown in Fig. 3C). Two models were simulated to verify this viewpoint. Model 1 is a system with 12 rigid coexisted with 12 flexible

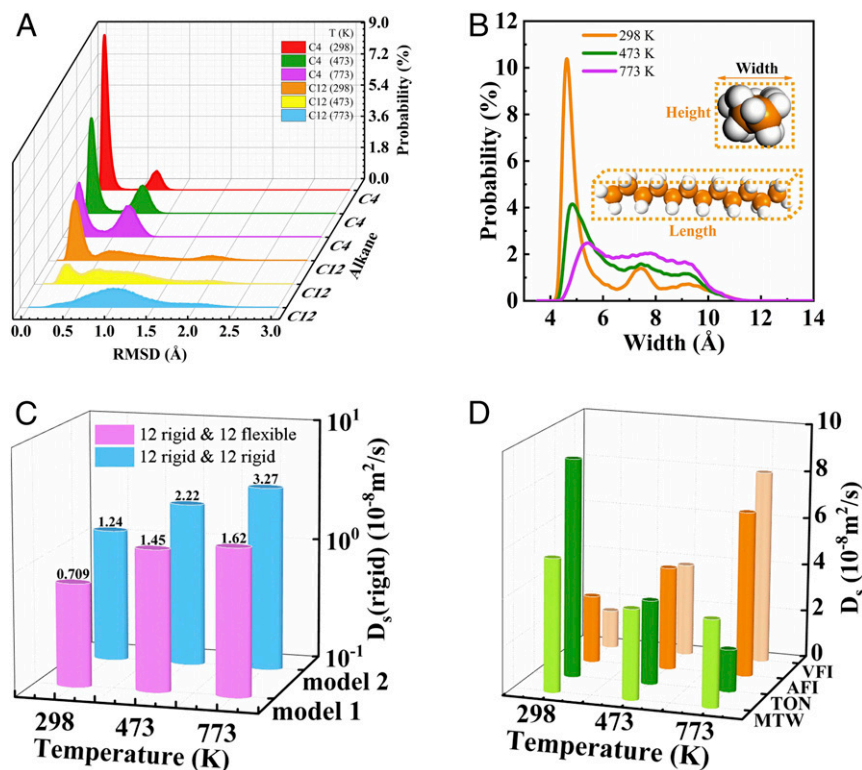


Fig. 3. (A) The RMSD of C4 and C12 molecule inside MFI zeolite. (B) The distribution of width for C12 molecule inside MFI zeolite at various temperatures. (C) Self-diffusion coefficient at different temperatures of 12 rigid C12 molecules in a system of 12 rigid and 12 flexible (blue), and 12 rigid and 12 rigid (pink). (D) Self-diffusion coefficients of C12 inside MTW, TON, AFI, and VFI zeolites.

molecule C12. Model 2 is another comparative system with 24 rigid C12. The D_s of the 12 rigid molecules of both systems are calculated for the determination of how the flexible and rigid molecules affect the diffusion of other structures. The former system with flexible skeleton owns a smaller D_s (for model 1, D_s is 0.71×10^{-8} [298 K], 1.45×10^{-8} [473 K], 1.62×10^{-8} [773 K] m^2/s) than the latter one (model 2, 1.24×10^{-8} [298 K], 2.22×10^{-8} [473 K], 3.27×10^{-8} [773 K] m^2/s) which only has a rigid configuration. Furthermore, a marginal difference of D_s between the two systems at low temperatures is exhibited (0.53×10^{-8} m^2/s at 298 K); however, the difference becomes significantly more obvious as the temperature increases (1.65×10^{-8} m^2/s at 773 K). More linear-chain molecules are present in the branched-like configuration at higher temperatures and consequently slow down the diffusion. In general, two kinds of resistance are seen for the deformed molecule in MFI zeolite during the diffusion process: hinder the diffusion of the molecules themselves (Fig. 2 B and C) and also restrain the diffusion of other molecules coadsorbed in the zeolite channels (Fig. 3C).

The temperature-induced deformation of the molecule shows a general trend for the gas molecule. However, there is no TRE to be observed in the gas phase even for the distorted (SI Appendix, Fig. S3D) molecules at high temperatures (SI Appendix, Table S2 and Fig. 2D). TRE is strongly correlated to the zeolite framework and its pore size. Therefore, we discussed the existence conditions of TRE of the diffusion in the zeolite systems. MTW, TON, AFI, and VFI are 1-D channel zeolite with a pore size of $5.6 \text{ \AA} \times 6.0 \text{ \AA}$, $4.6 \text{ \AA} \times 5.7 \text{ \AA}$, $7.3 \text{ \AA} \times 7.3 \text{ \AA}$, and $12.7 \text{ \AA} \times 12.7 \text{ \AA}$, respectively (SI Appendix, Fig. S1 B–E). TRE diffusion is only present in MTW and TON zeolite (Fig. 3D and SI Appendix, Table S2) whose pore size is similar to that of MFI. A normal behavior was obtained in the larger channel of AFI and VFI zeolite due to the weaker host–guest interactions between the distorted C12 and framework at high temperatures (SI Appendix, Fig. S3 and Fig. 4). Furthermore, the confinement effect in the zeolite can be qualitatively assessed by the scatter plot of the reduced density gradient (RDG) in real space (28). This is an effective and widely used tool to visualize noncovalent interactions between adsorbates and zeolite.

The RDG scatters are one kind of method to qualitatively describe the interaction in the host–guest system (29). As illustrated by RDG scatters of the *n*-C12 in MFI, MTW, and VFI at 298 K and 773 K in Fig. 5, the difference on RDG scatters at different

temperature was reflected in the range from -0.03 to 0.01 atomic unit (orange squares). Normally, the density of points at this range indicates the strength of the van der Waals (vdW) interaction, but the density of points out of this range indicates the strong intramolecular interaction (blue region) and intramolecular repulsive interaction (red region) under the premise of excluding these interactions between *n*-C12 and zeolites. Obviously, vdW interactions reveal different tendencies. For example, dodecane inside MFI and MTW at higher temperatures (Fig. 5 B and D) has a region with the higher density than that at lower temperatures (Fig. 5 A and C), which indicates a stronger interaction between C12 and MFI (or MTW) at high temperatures. The density of C12 in VFI is almost the same at both the low (Fig. 5E) and high temperatures Fig. 5F, which clearly illustrated that the variations of the temperature will lead to subtle changes in the interactions. Moreover, a less concentrated distribution of the RDG versus those of MFI and MTW show the lesser confinement effects of C12 inside VFI zeolite channel with large pore size, regardless of the degree of dodecane deformation with the temperature.

We also consider the effect of concentration (SI Appendix, Supplemental Material and Fig. S6) as well as other long chain molecules such as cetane and dodecatylene (SI Appendix, Table S2). This shows that this anomalous diffusion was also presented, which clearly illustrated the robustness of the TRE in the diffusion. In addition, the deformation of adsorbate was also confirmed by the ab initio MD (AIMD) simulation (SI Appendix, Fig. S7), which was able to capture the dynamic behavior of molecules more accurately (30). Moreover, the results of our ZLC experiments (SI Appendix, Fig. S8) also proved the existence of thermal resistance effect. Overall, the confinement effect of zeolite channels as well as high temperatures induced the distortion of long-chain molecules and will lead to a TRE.

Discussion

In summary, an anomalous effect for molecules diffusion dependent on temperature was observed whereby a higher temperature would induce a smaller diffusion coefficient of long-chain molecules (e.g., C12 and other longer chains hydrocarbon molecules) inside the confined channel of zeolite. This counterintuitive effect originates from the deformation of adsorbate as well as the increased confinement (i.e., host–guest interaction) results via the relatively bulky size under the higher temperature in the zeolite channels. Similar to the thermistor, this is a TRE in the diffusion

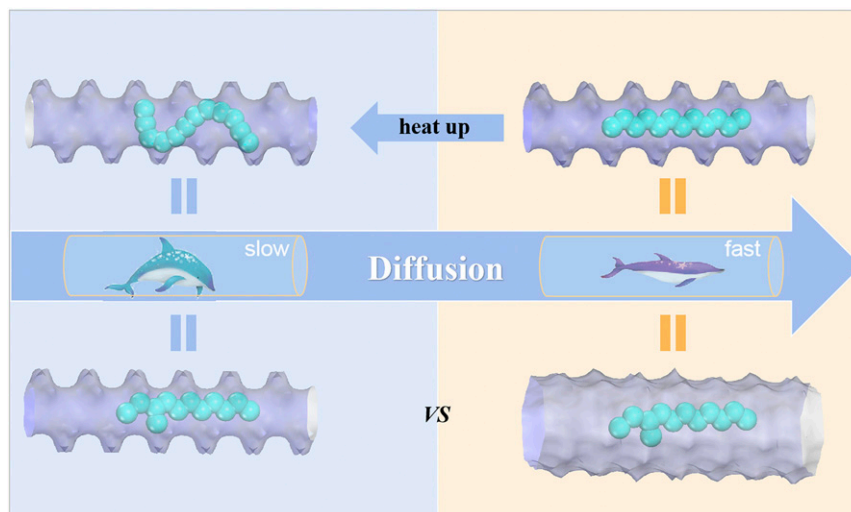


Fig. 4. The scheme of TRE for C12 molecule diffused inside zeolite channels at low and high temperatures. The diffusion resistance of linear-chain molecules at high temperatures is equivalent to that of the branched-chain configuration, which induces slow diffusion under confinement. There is no TRE for C12 in a large-size channel.

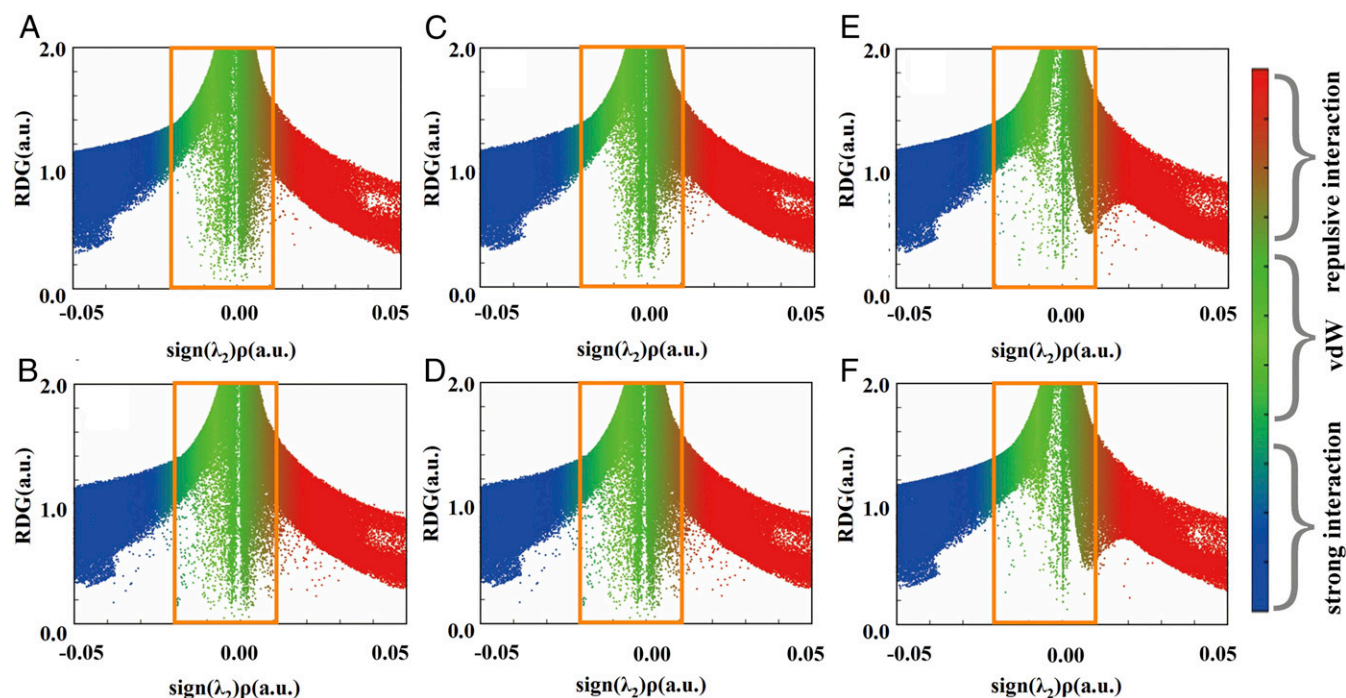


Fig. 5. The RDG scatter of dodecane in MFI (A and B), MTW (C and D), and VPI (E and F) zeolites at 298 K and 773 K, respectively..

behavior inside zeolite confined channels. This work will enrich our understanding of an anomalous mechanism of the diffusion phenomenon and could shed light on a fundamental understanding of the diffusion process.

Materials and Methods

MD Simulation. In our simulations, the initial structures of MFI, MTW, TON, AFI, and VFI were taken from the International Zeolite Associations (IZA) database (*SI Appendix*, Fig. S1) (31) and optimized by GULP (32) with SLC core-shell force field (33, 34). A $2 \times 2 \times 3$ supercell with the loading of 12 molecules (C4, C8, C12) was used for MFI, while larger $3 \times 3 \times 4$ supercell of MFI was performed for CH₄ (36 molecules) to avoid larger fluctuations in temperature. The $2 \times 10 \times 4$, $2 \times 2 \times 6$, $3 \times 3 \times 5$, and $3 \times 3 \times 6$ supercells with a loading of 16, 8, 9, and 9 C₁₂H₂₆ (n-dodecane) molecules were used for MTW, TON, AFI, and VFI, respectively. MD simulations were performed in the canonical ensemble (NVT), where the number of particles (N), volume (V), and temperature (T) were kept constant. The simulated temperature ranged from 298 K to 773 K (i.e., 298, 398, 473, 573, 673, and 773 K) as controlled by a Nosé-Hoover thermostat with a coupling time constant of 0.1 ps. For the molecules in condensed phase, the NPT ensemble (constant number of particles N, pressure P, and temperature T) was used for equilibration so that the volumes were stable at a pressure of 1 atm and various temperatures. The NVT ensemble was conducted to study the diffusion behaviors. The leapfrog Verlet algorithm was used to integrate Newton's equations of motion with a time step of 0.5 fs. The TraPPE-zeo (35) and TraPPE-UA (36) force field were used for zeolite and hydrocarbon, respectively. All the Lennard-Jones cross-interaction parameters were determined by the Lorentz-Berthelot mixing rules, and the cutoff radius was 14 Å. Each MD simulation was equilibrated for 2×10^6 steps, and then 4×10^7 steps of production were recorded for the research on the diffusion behaviors of adsorbate molecules. The trajectories were recorded every 1,000 steps, and three independent MD simulations were conducted for better statistics. All MD simulations were performed in the DL_POLY 2.0 code (37). The details of the AIMD calculations are presented in section 1.6 of the *SI Appendix*.

Diffusion Coefficient. In this work, the mean square displacement (MSD) of adsorbates is defined via the following equation:

$$MSD(\tau) = \frac{1}{N_m} \sum_i \frac{1}{N_\tau} \sum_{t_0}^{N_\tau} [r_i(t_0 + \tau) - r_i(t_0)]^2 \quad [2]$$

Here, N_m is the number of gas molecules, N_τ is the number of time origins used in calculating the average, and r_i is the coordinate of the i th molecule. In addition, the slope of the MSD as a function of time determines the self-diffusion coefficient (D_s) defined according to the so-called Einstein relationship (38):

$$MSD(\tau) = 2nD_s\tau + b, \quad [3]$$

where n is the dimension of frameworks ($n = 1$ for 1-D diffusion, i.e., along the X, Y, and Z in MFI, as well as in 1-D MTW, TON, AFI, and VFI zeolites; $n = 3$ for MFI and in gas phase). The diffusion coefficients were obtained by fitting the linear region of MSD using a least-square fit. The D_s values were calculated as the average of three dependent MD trajectories.

ZLC Measurements. The ZLC setup was similar to the apparatus reported by Shiran et al. (39). The ZLC and switching valve were placed in Bruker 450 GC oven to ensure that the system had a constant temperature. The effluent gas stream was continuously monitored with the flame ionization detector detector of the same gas chromatography. Here, 5.0 mg silicalite-zeolite was pretreated at 300 °C for 5 h to remove moisture and residual impurities. It was then cooled to the desired temperature. The partial pressures of n-dodecane and n-butane are 0.31 and 0.27 kPa, respectively. The desorption measurements were performed by purging with pure nitrogen at the same flow rate. Further details are provided in the *SI Appendix*.

Data Availability. All study data are included in the article and/or *SI Appendix*.

ACKNOWLEDGMENTS. This work is supported by the National Natural Science Foundation of China (22032005, 21902180, 21802164, 21991092, 21991090, 22002174 and 91645112), and the Natural Science Foundation of Hubei Province of China (2018CFA009), the Key Research Program of Frontier Sciences, Chinese Academy of Sciences (QYZDB-SSW-SLH026), and Sinopec Corp. (417012-4). We are grateful to the Shenzhen Cloud Computing Center for their support in computing facilities.

1. A. Bunde, J. Caro, J. Karger, G. Vogl, *Diffusive Spreading in Nature. Technology and Society* (Springer, 2018), pp. 313–331.
2. P. Cnudde et al., Light olefin diffusion during the MTO process on H-SAPO-34: A complex interplay of molecular factors. *J. Am. Chem. Soc.* **142**, 6007–6017 (2020).

3. C. Gu et al., Design and control of gas diffusion process in a nanoporous soft crystal. *Science* **363**, 387–391 (2019).
4. P. J. Bereciartua et al., Control of zeolite framework flexibility and pore topology for separation of ethane and ethylene. *Science* **358**, 1068–1071 (2017).

5. B. Smit, T. L. M. Maesen, Molecular simulations of zeolites: Adsorption, diffusion, and shape selectivity. *Chem. Rev.* **108**, 4125–4184 (2008).
6. K. Hahn, J. Kärger, V. Kukla, Single-file diffusion observation. *Phys. Rev. Lett.* **76**, 2762–2765 (1996).
7. V. Gupta, S. S. Nivarthi, D. Keffer, A. V. McCormick, H. T. Davis, Evidence of single-file diffusion in zeolites. *Science* **274**, 164 (1996).
8. V. Kukla *et al.*, NMR studies of single-file diffusion in unidimensional channel zeolites. *Science* **272**, 702–704 (1996).
9. Q. Wei, C. Bechinger, P. Leiderer, Single-file diffusion of colloids in one-dimensional channels. *Science* **287**, 625–627 (2000).
10. E. G. Derouane, J.-M. André, A. A. Lucas, Surface curvature effects in physisorption and catalysis by microporous solids and molecular sieves. *J. Catal.* **110**, 58–73 (1988).
11. S. Nag, G. Ananthakrishna, P. K. Maiti, S. Yashonath, Separating hydrocarbon mixtures by driving the components in opposite directions: High degree of separation factor and energy efficiency. *Phys. Rev. Lett.* **124**, 255901 (2020).
12. D. Dubbeldam, S. Calero, T. L. M. Maesen, B. Smit, Incommensurate diffusion in confined systems. *Phys. Rev. Lett.* **90**, 245901 (2003).
13. R. L. Goring, Diffusion of normal paraffins in zeolite-T-occurrence of window effect. *J. Catal.* **31**, 13–17 (1973).
14. E. G. Derouane, Z. Gabelica, A novel effect of shape selectivity-molecular traffic control in zeolite ZSM-5. *J. Catal.* **65**, 486–489 (1980).
15. E. Ruckenstein, P. S. Lee, Resonant diffusion. *Phys. Lett. A* **56**, 423–424 (1976).
16. R. C. Runnebaum, E. J. Maginn, Molecular dynamics simulations of alkane in the zeolite silicalite: Evidence for resonant diffusion effects. *J. Phys. Chem. B* **101**, 6394–6408 (1997).
17. D. Dubbeldam, S. Calero, T. L. M. Maesen, B. Smit, Understanding the window effect in zeolite catalysis. *Angew. Chem. Int. Ed. Engl.* **42**, 3624–3626 (2003).
18. D. Dubbeldam, E. Beersden, S. Calero, B. Smit, Molecular path control in zeolite membranes. *Proc. Natl. Acad. Sci. U.S.A.* **102**, 12317–12320 (2005).
19. S. Gao *et al.*, Cavity-controlled diffusion in 8-membered ring molecular sieve catalysts for shape selective strategy. *J. Catal.* **377**, 51–62 (2019).
20. J. Kärger, H. Pfeifer, F. Stallmach, N. N. Feoktistova, S. P. Zhdanov, ¹²⁹Xe and ¹³C PFG NMR study of the intracrystalline self-diffusion of Xe, CO₂, and CO. *Zeolite* **13**, 50–55 (1993).
21. A. Ghysels *et al.*, Shape-selective diffusion of olefins in 8-ring solid acid microporous zeolite. *J. Phys. Chem. C* **119**, 23721–23734 (2015).
22. E. Beersden, B. Smit, Diffusion in confinement: Agreement between experiments better than expected. *J. Phys. Chem. B* **110**, 14529–14530 (2006).
23. D. Zhong *et al.*, Linear alkane polymerization on a gold surface. *Science* **334**, 213–216 (2011).
24. H. Jobic, W. Schmidt, C. B. Krause, J. Karger, PFG NMR and qens diffusion study of N-alkane homologues in MFI-type zeolite. *Microporous Mesoporous Mater.* **90**, 299–306 (2006).
25. H. Jobic, Diffusion of linear and branched alkane in ZSM-5. A quasi-elastic neutron scattering study. *J. Mol. Catal. Chem.* **158**, 135–142 (2000).
26. F. Leroy, B. Rousseau, Self-diffusion of N-alkane in MFI type zeolite using molecular dynamics simulations with an anisotropic united atom (AUA). *Forcefield. Mol. Simulat.* **30**, 617–620 (2004).
27. K. Hahn, J. Karger, Molecular dynamics simulation of single-file systems. *J. Phys. Chem.* **100**, 316–326 (1996).
28. E. R. Johnson *et al.*, Revealing noncovalent interactions. *J. Am. Chem. Soc.* **132**, 6498–6506 (2010).
29. W. Li, M. M. Quesada-moreno, P. Pinacho, M. Schnell, Unlocking the water trimer loop: Isotopic study of benzophenone-(H₂O)₁₋₃ clusters with rotational spectroscopy. *Angew. Chem. Int. Edit.* **133**, 5383–5390 (2021).
30. X. Tang *et al.*, Violation or abidance of Löwenstein's rule in zeolites under synthesis conditions? *ACS Catal.* **9**, 10618–10625 (2019).
31. C. Baerlocher, L. B. McCusker, Database of zeolite structures. www.izastructure.org/databases/. (Accessed Jun 2016).
32. J. D. Gale, A. L. Rohl, The general utility lattice program, (Gulp). *Mol. Simul.* **29**, 291–341 (2003).
33. C. R. A. Catlow, C. M. Freeman, B. Vessal, S. M. Tomlinson, M. Leslie, Molecular-dynamics studies of hydrocarbon diffusion in zeolite. *J. Chem. Soc., Faraday Trans.* **87**, 1947–1950 (1991).
34. M. J. Sanders, M. Leslie, C. R. A. Catlow, Interatomic potentials for SiO₂. *J. Chem. Soc. Chem. Comm.* **19**, 1271–1273 (1984).
35. P. Bai, M. Tsapatsis, J. I. Siepmann, Trappe-Zeo: Transferable potentials for phase equilibria force field for all-silica zeolite. *J. Phys. Chem. C* **117**, 24375–24387 (2013).
36. C. D. Wick, M. G. Martin, J. I. Siepmann, Transferable potentials for phase equilibria. 4. United-atom description of linear and branched alkenes and alkylbenzenes. *J. Phys. Chem. B* **104**, 8008–8016 (2000).
37. W. Smith, T. R. Forester, DL_POLY_2.0: A general-purpose parallel molecular dynamics simulation package. *J. Mol. Graph.* **14**, 136–141 (1996).
38. D. Frenkel, B. Smit, *Understanding Molecular Simulations* (Elsevier, Singapore, 2002).
39. B. Shirani, X. Han, M. Eic, Application of ZLC technique for a comprehensive study of hydrocarbons kinetics in carbon molecular sieves and zeolites. *Separ. Purif. Tech.* **230**, 115831 (2020).



Supplementary Information for

Thermal resistance effect on anomalous diffusion of molecules under confinement

Jiamin Yuan ^{a,b}, Zhiqiang Liu ^{a,*}, Yimo Wu ^{b,c}, Jingfeng Han ^c, Xiaomin Tang ^{a,b}, Chengbin Li ^a, Wei Chen ^a, Xianfeng Yi ^a, Jian Zhou ^d, Rajamani Krishna ^e, German Sastre ^f, Anmin Zheng ^{a,*}.

^a State Key Laboratory of Magnetic Resonance and Atomic and Molecular Physics, National Center for Magnetic Resonance in Wuhan, Wuhan Institute of Physics and Mathematics, Innovation Academy for Precision Measurement Science and Technology, Chinese Academy of Sciences, 430071 Wuhan, China.

^b University of Chinese Academy of Sciences, 100049 Beijing, China.

^c National Engineering Laboratory for Methanol to Olefins, State Energy Low Carbon Catalysis and Engineering R&D Center, Dalian National Laboratory for Clean Energy, iChEM (Collaborative Innovation Center of Chemistry for Energy Materials), Dalian Institute of Chemical Physics, Chinese Academy of Sciences, 116023 Dalian, Liaoning, China.

^d Shanghai Research Institute of Petrochemical Technology, SINOPEC, 201208 Shanghai, China.

^e Van't Hoff Institute for Molecular Sciences, University of Amsterdam, 1098 XH Amsterdam, The Netherlands.

^f Instituto de Tecnología Química, Consejo Superior de Investigaciones Científicas, Universitat Politècnica de Valencia, 46022 Valencia, Spain.

This PDF file includes:

Supplementary text
Figures S1 to S9
Tables S1 to S3
SI References

Supplementary Information Text

1. Methods and text

1.1 Distribution of distorted angle

The distorted angle of the molecule is calculated from the deviation of the angle along the (i-2)th, (i)th and (i+2)th carbon atoms from equilibrium angle 180°. For example, there are eight (*i.e.*, n-4: n = 12 for dodecane) different angles (*i.e.*, 1-3-5, 2-4-6, 3-5-7, 4-6-8, 5-7-9, 6-8-10, 7-9-11, 8-10-12) for a dodecane molecule. As is depicted in Fig. S2, the deviation of the angle $\angle 1$ is following equation (1), where $\angle 2$ represents the variable angle for the (i-2)th, (i)th and (i+2)th carbon atoms. Then, the number of occurrences for a maximal $\angle 1$ of each molecule at various temperatures is counted, which indicates the degree of molecular bending and reflects the flexibility of the molecule in the confined channel at different temperatures.

$$\angle 1 = |180^\circ - \angle 2| \quad (1)$$

Besides C12, a long chain alkane like C8 also exhibits distortion (Fig. S3(a)). Therefore, the diffusion of C8 was influenced by the TRE as well. Furthermore, for the diffusion of C12 inside zeolite MTW (Fig. S3(b)), AFI (Fig. S3(c) and Fig.S9(a)) and VFI (Fig. S3(c) and Fig.S9(b)), molecular distortions also exist. This shows that the anomalous diffusion is presented in MTW (with a pore size similar to MFI), while it has not been observed in VFI zeolite with large pore size (12.7 Å × 12.7 Å) due to less confinement, which allows molecules to diffuse freely.

It should be noted that the diffusivities of C12 still slightly decrease at 700/800 K (see Figure 1b), but the change trend is not as notable as that at 300~600 K. At low temperatures, the increase in temperature is accompanied by an obvious bending phenomenon, and thus the diffusivities decrease remarkable. However, as the temperature rises to a certain temperature, such as 600 K, and then the deformation of molecule is not as large as that at low temperature (see Figure 2a). And therefore, the decrease in diffusion coefficient is less obvious at 700/800K.

1.2 Root-mean-square deviation (RMSD)

Quantitative comparison of molecular structures deformation at different temperatures is of great importance, the root-mean-square deviation (RMSD) of the Cartesian positions of the equivalent atoms in two structures (the reference configuration and the transient one) is regarded as a standard measure for the molecular deformation [1]. Before RMSD calculation, it is necessary to use a rigid body translation and rotation of one structure with respect to the other by a least-squares superposition procedure [2]. Molecular dynamics (MD) trajectories of C4 and C12 are analyzed by comparison of each molecule at each step under various temperatures with respect to a reference structure. Finally, the probability of each RMSD value at different temperatures is calculated. The calculation of RMSD is performed by visual molecular dynamics (VMD) package [3]. In this work, the root-mean-square deviation of adsorbate is defined as the following equation:

$$RMSD = \sqrt{\frac{\sum_{i=1}^{N_{atoms}} [r_i(t_1) - r_i(t_2)]^2}{N_{atoms}}} \quad (2)$$

where N_{atoms} is the number of atoms, r_i is the position of atom i at time t [1].

1.3 Reduced density gradient (RDG) analysis

Confinement effect in zeolite can be assessed by qualitative method, the scatter plot of the reduced density gradient (RDG) in real space is an effective and widely used tool to visualize non-covalent interaction between adsorbates and zeolite [4]. A random frame during the molecular dynamic simulation was selected to plot the RDG scatter as well as structures and dominant intermolecular interactions for the description of the host-guest interaction between the adsorbate and framework. The non-covalent interaction was performed in the region with low density and the RDG is defined as [4]

$$s = \frac{1}{2(3\pi^2)^{1/3}} \times \left(\frac{|\Delta\rho(r)|}{\rho(r)^{4/3}} \right) \quad (3)$$

together with the electron density ρ , which is used to distinguish the interaction (covalent and non-covalent). Hessian can be used to distinguish bonded ($\lambda_2 < 0$) from non-bonded ($\lambda_2 > 0$) interaction for the sign of the second largest eigen-value (λ_2) of the electron density. This helps to distinguish different types of interactions ($(\lambda_2)\rho < 0$, strong intramolecular interaction; $(\lambda_2)\rho \approx 0$, weak van der Waals (vdW) interaction; $(\lambda_2)\rho > 0$, strong repulsive interaction). To reveal the confinement effect more precisely, the inter-molecular interaction was adapted for the RDG analysis. The RDG function was calculated by Multiwfn [5].

1.4 The calculation of the shape for molecule inside zeolite

The length, width and height of a molecule, which calculated from the difference between the maximum and the minimum coordinate of a molecule at each direction (*i.e.* x, y and z) (The van der Waals radius is taken into account), can be used to interpret the anomalous diffusion behavior of n-alkane inside zeolite. In this work, the length, width and height follow the order of length > width > height, and three values are defined as formula (4) to (9). Where 1.7 Å represents the van der Waals radius of atom C. X_{max}/X_{min} (Y_{max}/Y_{min} or Z_{max}/Z_{min}) is the maximum/minimum coordinate of the atom inside the C12 molecule at different directions. Corresponding schematic diagram for the definition of the molecular length, width and height is shown in Fig. S4.

$$X_{max} - X_{min} = a \quad (4)$$

$$Y_{max} - Y_{min} = b \quad (5)$$

$$Z_{max} - Z_{min} = c \quad (6)$$

$$\text{Length} = \text{maximum}(a, b, c) + 1.7 \times 2 \quad (7)$$

$$\text{Width} = \text{median}(a, b, c) + 1.7 \times 2 \quad (8)$$

$$\text{Height} = \text{minimum}(a, b, c) + 1.7 \times 2 \quad (9)$$

As is depicted in Fig. S5 (a), the length of C12 inside MFI zeolite is mainly distributed at 17.6 Å at 298 K, while owns a wider range at 473 K (mainly from 15.5 to 17.7 Å) and 773 K (mainly from 13.5 to 16.9 Å). It is more likely to find a shorter C12 with increasing temperature due to the molecular bending, and it is found that the width (Figure 3(b)) and height (Fig. S5 (b)) increase correspondingly as the length decreases. The probability of find a larger value of height at various temperatures follows the order that $P_{773\text{ K}} > P_{473\text{ K}} > P_{298\text{ K}}$. which demonstrated that the higher the temperature, the more molecules get fatter. It is more difficult for a fat molecule to pass through the same channel than a slim one. This conclusion is consistent with the diffusion coefficients listed Table S1.

1.5 Zero length column (ZLC) measurements

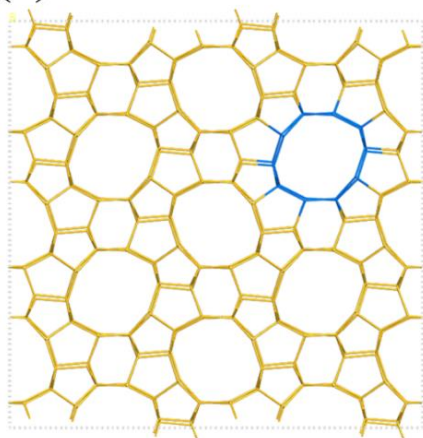
The ZLC setup was similar to the apparatus reported by Shirani [6]. The ZLC column and switching valve were placed in Bruker 450 GC oven to ensure the system temperature constant. The effluent gas stream was continuously monitored with the FID detector of the same gas chromatography. 5.0 mg silicalite-1 zeolite was pretreated at 300 °C for 5 hours to remove moisture and residual impurities, then cooling down to the desired temperature. Prior to desorption measurement, the sample was fully equilibrated with n-dodecane or n-butane diluted in a nitrogen flow of 80 ml/min at different temperatures. The partial pressure of n-dodecane and n-butane is 0.31 kPa and 0.27 kPa, respectively. The desorption measurements were performed by purging with pure nitrogen at the same flow rate. It is found that the thermal resistance effect also appears by ZLC experiments for C12 (the diffusion coefficient decreases with increasing temperature) (Fig. S8 (b)), and no TRE is observed for C4 inside MFI (diffusion trend opposite to C12) (Fig. S8 (a)). These results were consistent with our MD simulations.

1.6 *Ab initio* molecular dynamics (AIMD)

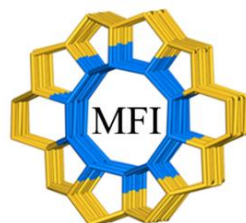
The periodic density functional theory (DFT) as well as the advanced *ab initio* molecular dynamics (AIMD) simulation were performed using the CP2K [7-9] package. The MFI framework was obtained from the IZA database [10] and fully relaxed with unit cell parameters $a = 20.316 \text{ \AA}$, $b = 19.941 \text{ \AA}$, $c = 13.373 \text{ \AA}$, and $\alpha = \beta = \gamma = 90.0^\circ$. The MFI-dodecane (C12) complexes were cell optimized, and then, three 20 ps AIMD simulations in NVT ensemble were carried out for MFI-C12 complex at 298 K, 473 K, and 773 K. A Nosé-Hoover thermostat [11] with a time constant of 100 fs and a time step of 0.5 fs was employed during the AIMD process. All the calculations were carried out using the Perdew-Burke-Ernzerhof (PBE) exchange-correlation functional [12] in conjunction with Grimme's D3 correction [13] with zero damping to account for dispersion interactions. The DZVP basis set and GTH [14] pseudo potentials were chosen for all elements. The plane wave cutoff energy and relative cutoff was 650 Ry and 60 Ry, respectively. The structural distortion of C12 inside MFI is also calculated by AIMD trajectory for further verification of TRE. As shown in Fig. S7, the molecular bending angle was small at 298 K, but larger at 473 K and 773 K, indicating the deformation of C12 inside MFI at high temperatures.

2. Figures.

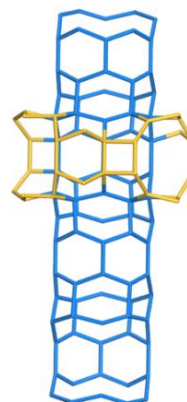
(a)



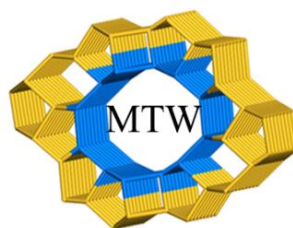
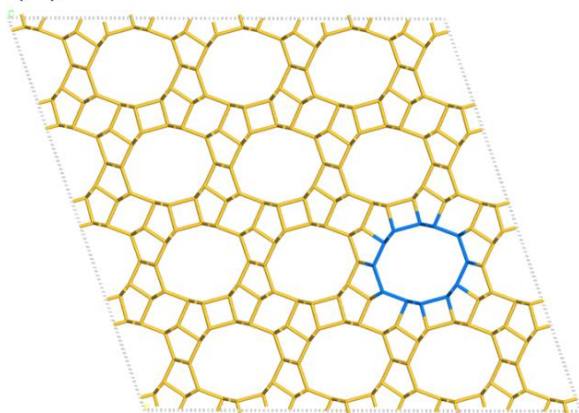
$5.1 \times 5.5 \text{ \AA}$



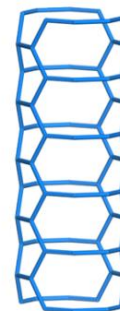
$5.3 \times 5.6 \text{ \AA}$



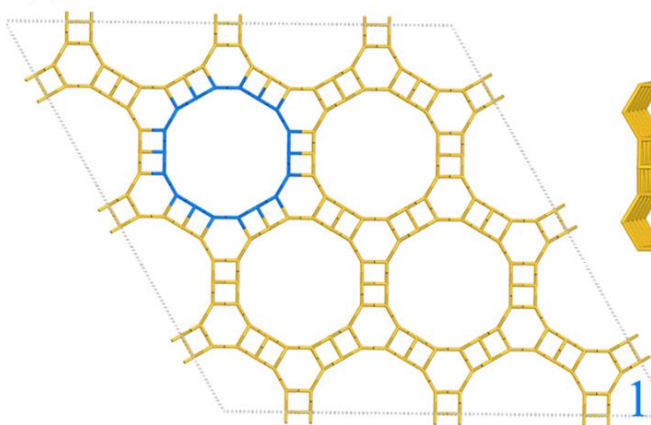
(b)



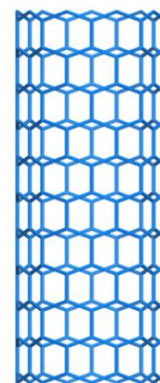
$5.6 \times 6.0 \text{ \AA}$



(c)



$12.7 \times 12.7 \text{ \AA}$



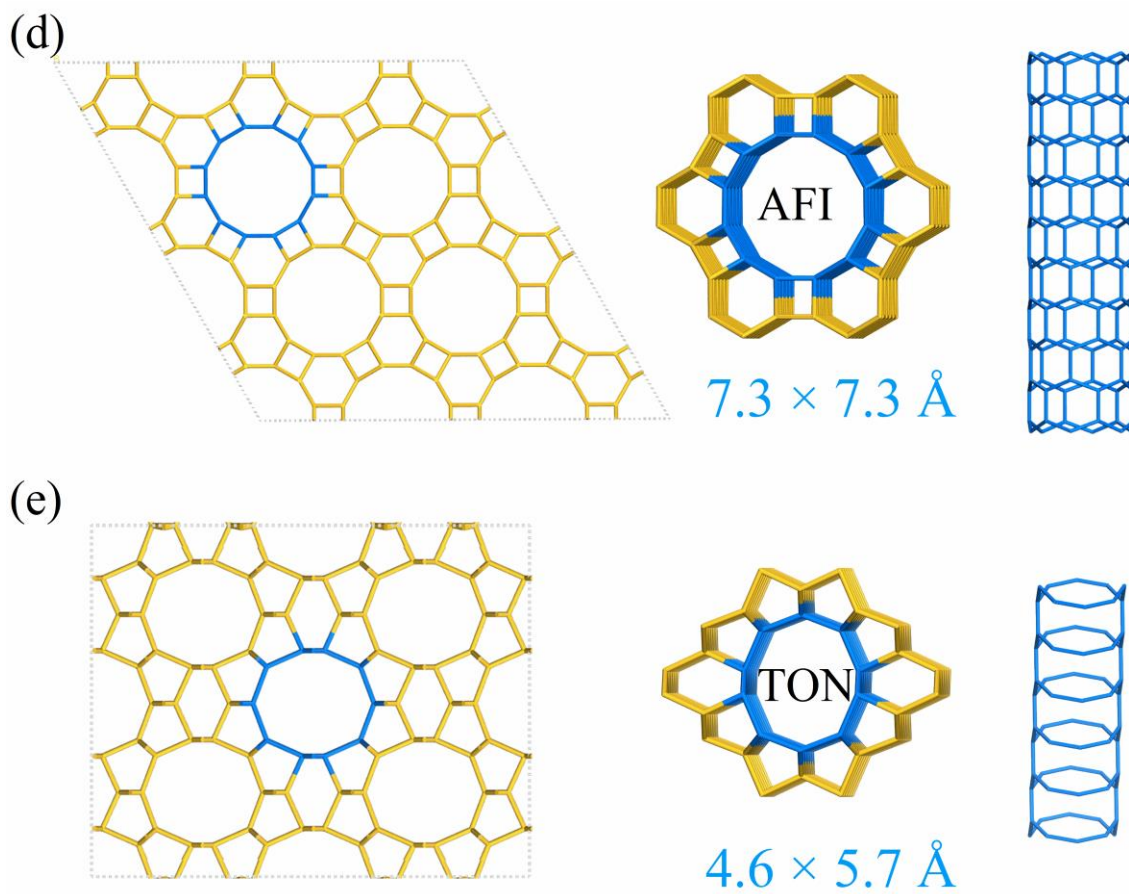


Fig. S1. The structure and channel of (a) MFI, (b) MTW, (c) VFI, (d) AFI, and (e) TON zeolites.

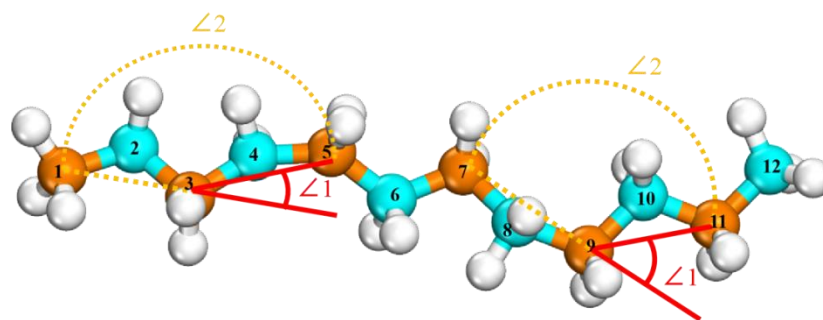


Fig. S2. The diagram of bending angle for dodecane.

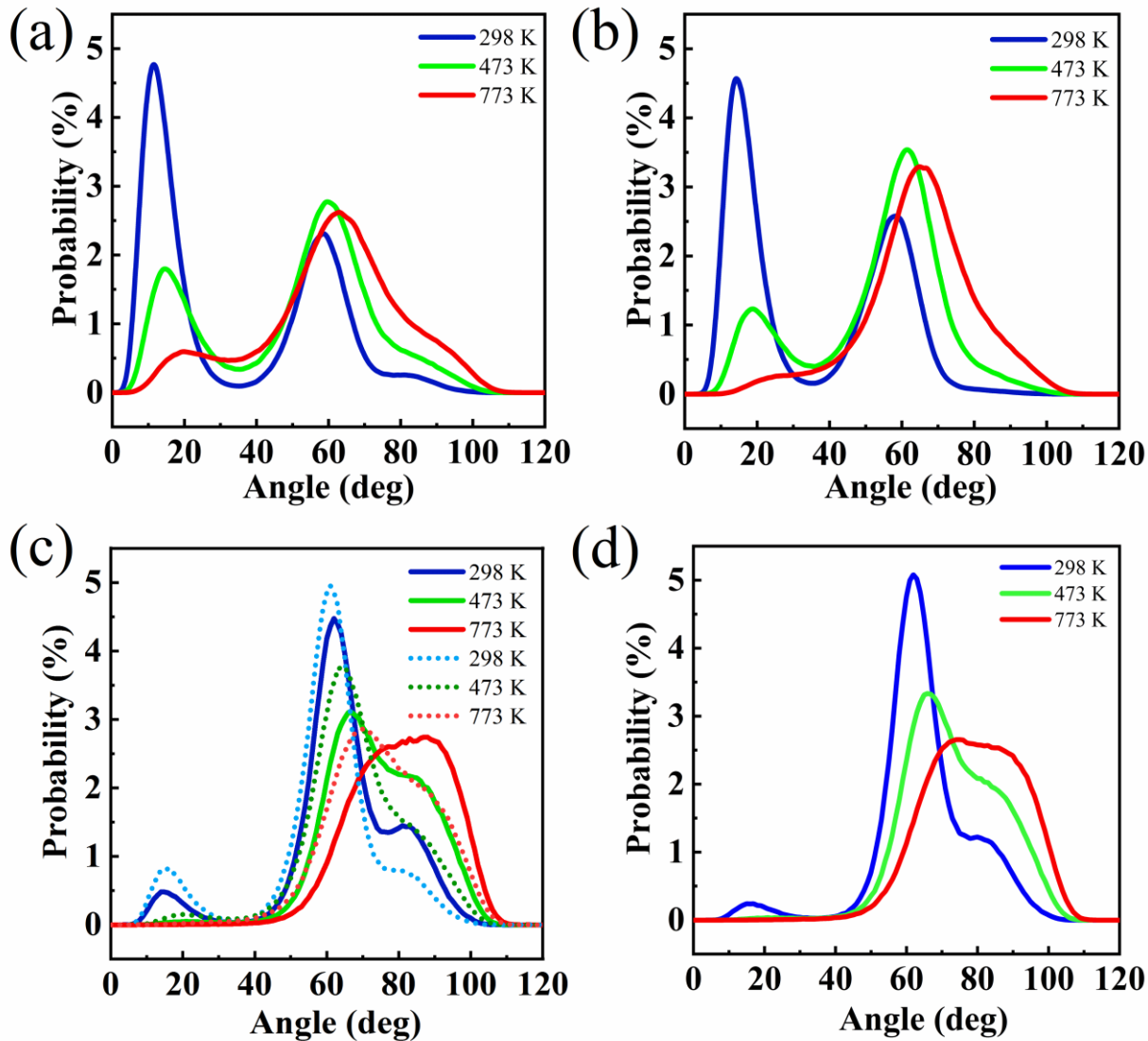


Fig. S3. (a) Distribution of distorted angle for C8 inside MFI. Distribution of distorted angle for C12 inside (b) MTW, (c) VFI (full line) and AFI (dash line) zeolite (d) gas phase at 298, 473 and 773 K.

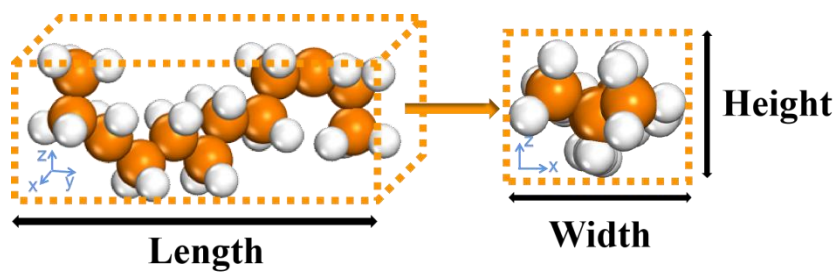


Fig. S4. Definition of the molecule length, width and height.

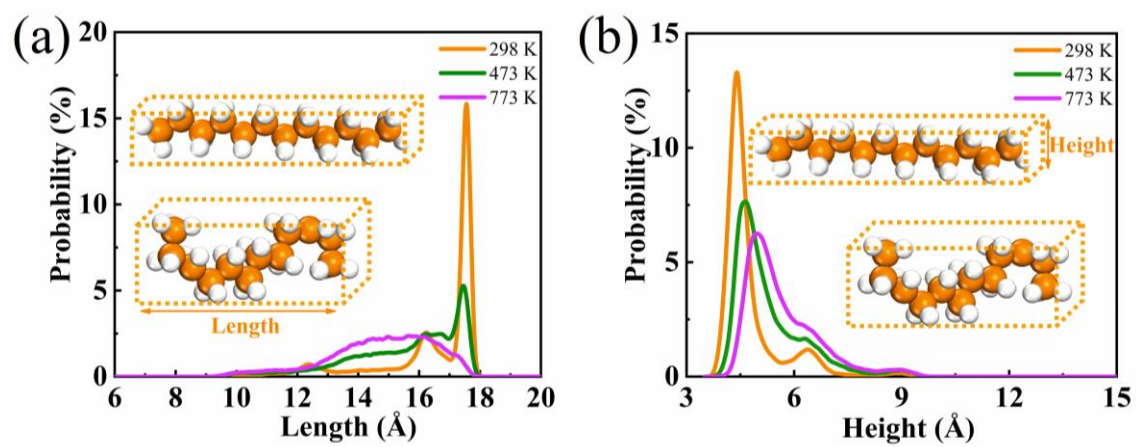


Fig. S5. The distribution of (a) length and (b) height of C12 inside MFI zeolite at different temperatures.

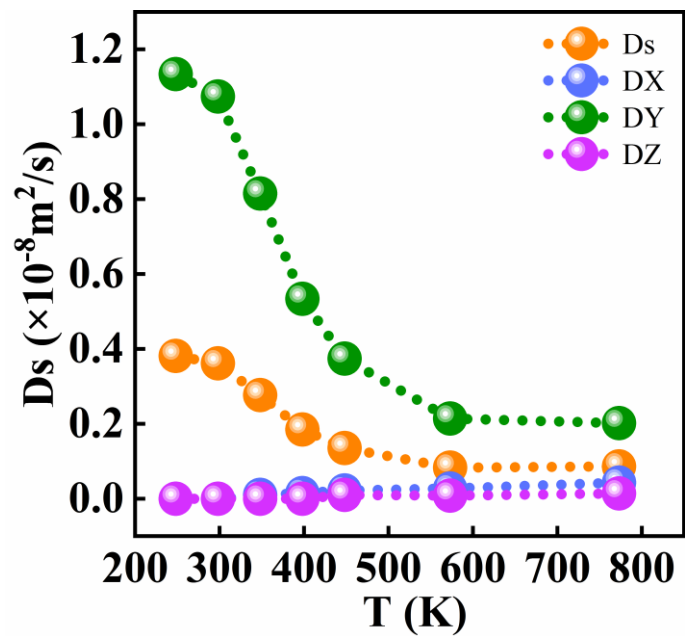


Fig. S6. The diffusion coefficient of C12 in MFI at high concentration.

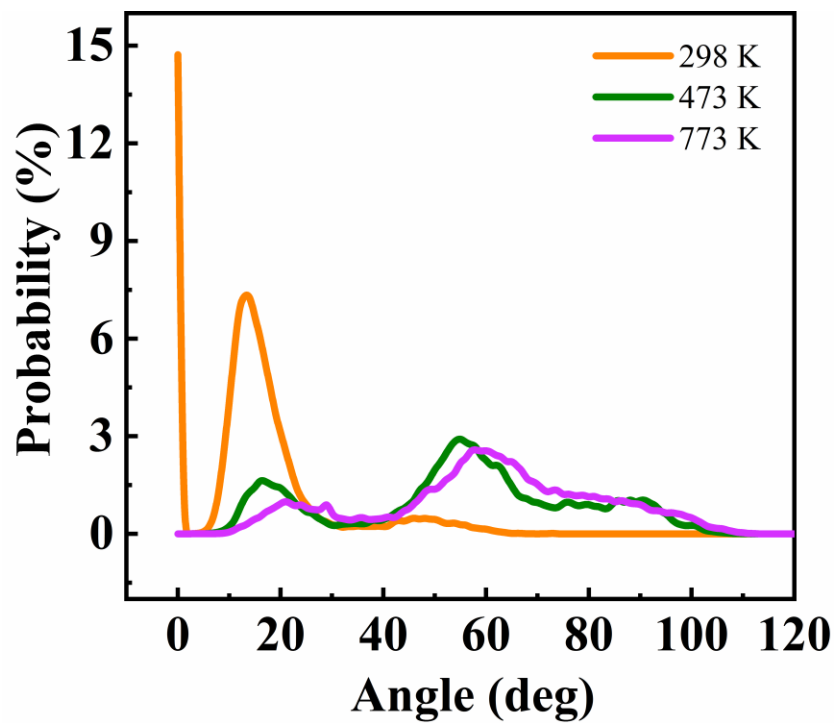


Fig. S7. Distribution of distorted angle for C12 inside MFI calculated by AIMD at different temperatures.

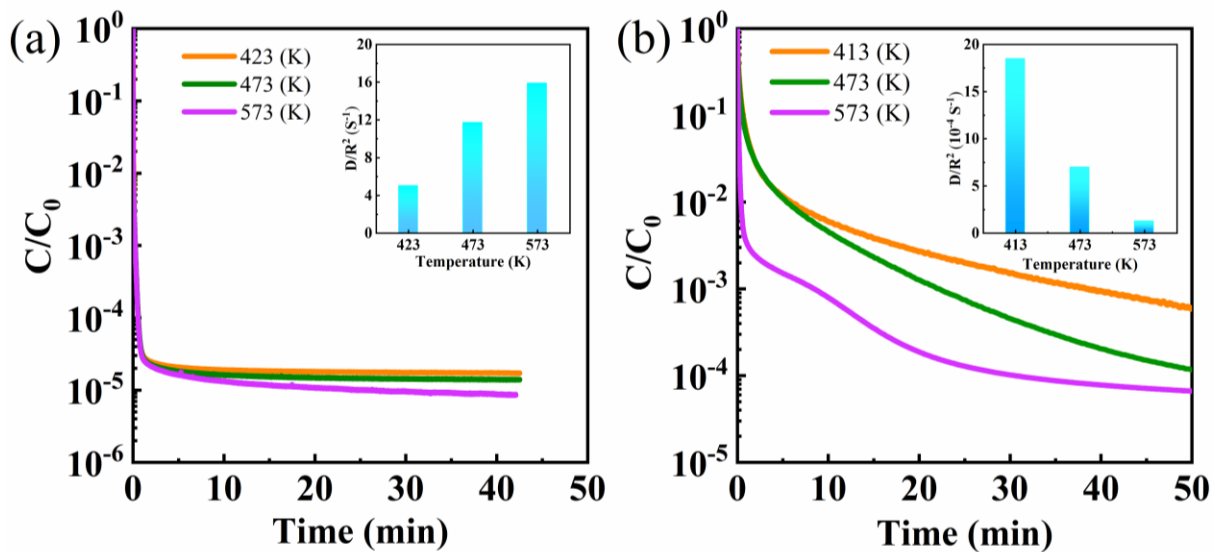


Fig. S8. The zero length column (ZLC) experiment desorption data of (a) n-butane and (b) n-dodecane for 5 mg zeolite at different temperatures and corresponding diffusion coefficients (inset).

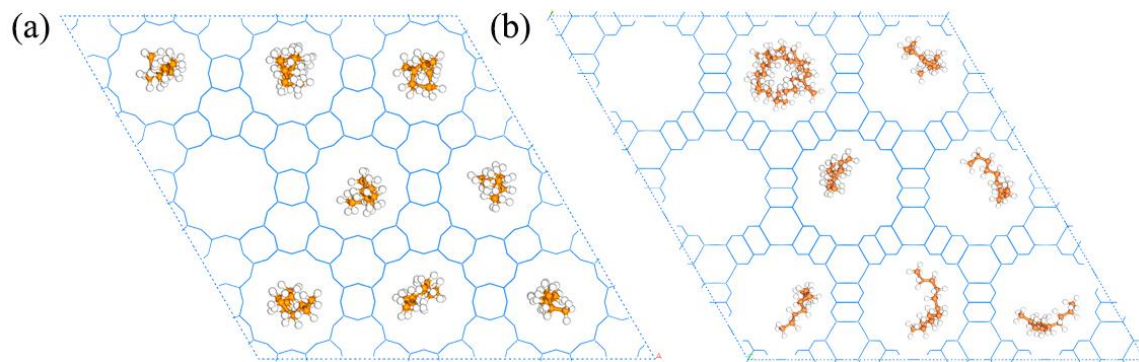


Fig. S9. The Snapshots of n-dodecane in (a) AFI and (b) VFI at 298 K.

3. Tables.

Table S1. Diffusion coefficients of alkane in MFI at different temperatures.

Diffusion coefficients of alkane in MFI ($\times 10^{-8}$ m ² /s)					
Temperature(K)	<i>D</i>	Alkane ^a			
		C1	C4	C8	C12
298	<i>D_X</i>	1.21	0.23	0.02	---
	<i>D_Y</i>	2.45	0.77	1.05	2.29
	<i>D_Z</i>	0.25	0.06	0.01	---
	<i>D_s</i>	1.30	0.35	0.36	0.76
	<i>D_X</i>	1.61	0.32	0.04	0.01
398	<i>D_Y</i>	3.33	0.78	1.00	1.16
	<i>D_Z</i>	0.34	0.09	0.02	---
	<i>D_s</i>	1.76	0.39	0.35	0.39
	<i>D_X</i>	2.09	0.35	0.08	0.02
473	<i>D_Y</i>	4.15	0.83	0.95	0.84
	<i>D_Z</i>	0.40	0.09	0.02	0.01
	<i>D_s</i>	2.21	0.42	0.35	0.29
	<i>D_X</i>	2.35	0.44	0.11	0.04
573	<i>D_Y</i>	4.85	0.86	0.90	0.49
	<i>D_Z</i>	0.45	0.10	0.04	0.01
	<i>D_s</i>	2.55	0.47	0.35	0.18
	<i>D_X</i>	2.82	0.50	0.14	0.06
673	<i>D_Y</i>	5.50	0.90	0.81	0.37
	<i>D_Z</i>	0.53	0.12	0.05	0.02
	<i>D_s</i>	2.95	0.50	0.33	0.15
	<i>D_X</i>	3.09	0.50	0.18	0.06
773	<i>D_Y</i>	5.87	0.90	0.90	0.36
	<i>D_Z</i>	0.59	0.12	0.06	0.02
	<i>D_s</i>	3.18	0.51	0.38	0.15
	<i>D_X</i>	3.09	0.50	0.18	0.06

^a C1 to C12 represents the alkane from methane to dodecane, *D_s* is the self-diffusion coefficients, *D_X*, *D_Y* and *D_Z* are the self-diffusion coefficients of alkane along different directions (X, Y, Z) in MFI.

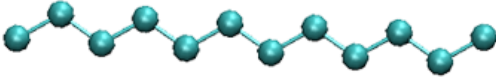
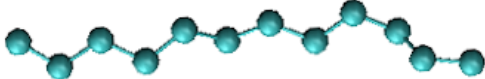
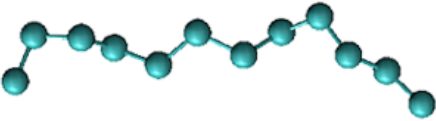
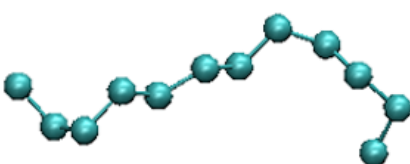
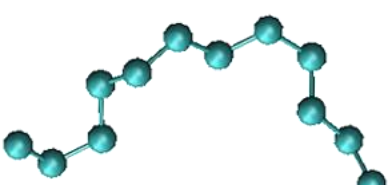
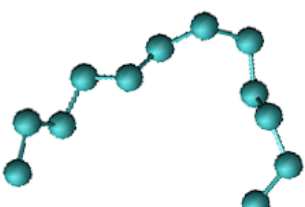
Table S2.Diffusion coefficients (D (10^{-8} m²/s)) of long chain molecules at various phase.

T (K)	D	MTW (C12)	VFI (C12)	TON (C12)	AFI (C12)	MFI (dodecatylene)) ^a	Condensed phase(C12)	MFI (C16)
298	D_x	---	---	---	---	---	0.13	---
	D_y	5.58	---	---	---	1.11	0.13	2.68
	D_z	---	1.60	9.16	2.83	---	0.13	---
	D_s	5.58	1.60	9.16	2.83	0.37	0.13	0.90
473	D_x	---	---	---	---	0.03	14.88	0.01
	D_y	3.78	---	---	---	0.64	15.59	1.00
	D_z	---	3.88	3.53	4.32	0.01	15.64	---
	D_s	3.78	3.88	3.53	4.32	0.23	15.37	0.34
773	D_x	---	---	---	---	0.08	35.66	0.05
	D_y	3.66	---	---	---	0.46	35.71	0.41
	D_z	---	8.10	1.78	6.93	0.03	32.92	0.02
	D_s	3.66	8.10	1.78	6.93	0.19	34.76	0.16

^a As seen in Table S2, for long-chain olefins like dodecatylene and cetane, the D_s inside MFI also under the influence of the TRE. The lower temperature causes the higher diffusion coefficient.

Table S3.

Typical deformed structure of dodecane (C12) with varied RMSD values.

RMSD (Å)	C12
0	
0.5	
1	
1.5	
2	
2.5	

4. SI References

- [1] R. Bruschweiler, Efficient RMSD Measures for the Comparison of Two Molecular Ensembles. *Proteins*. 50, 26-34 (2003).
- [2] R. Diamond, On the Comparison of Conformations Using Linear and Quadratic Transformations. *Acta Crystallogr*, A32, 1-10 (1976).
- [3] W. Humphrey, A. Dalke, K. Schulten, VMD: Visual Molecular Dynamics. *J. Mol. Graph.* 14, 33-38 (1996).
- [4] M. del C. Jorge, L. G. José, J. A -M. Rodrigo and V. Alberto, The Reduced Density Gradient in Atoms. *Int. J. Quantum Chem.* 112, 3594-3598 (2012).
- [5] T. Lu and F. Chen, Multiwfn: A Multifunctional Wavefunction Analyzer. *J. Comput. Chem.* 33, 580-592 (2012).
- [6] B. Shirani, X. Han and M. Eic, Application of ZLC Technique for a Comprehensive Study of Hydrocarbons Kinetics in Carbon Molecular Sieves and Zeolites. *Sep. Purif. Technol.* 230, 115831 (1-12) (2020).
- [7] J. Vandevondele, M. Krack, F. Mohamed, M. Parrinello, T. Chassaing, J. Hutter, Quickstep: Fast and Accurate Density Functional Calculations Using a Mixed Gaussian and Plane Waves Approach. *Comput. Phys. Commun.* 167, 103-128 (2005).
- [8] J. Vandevondele, J. Hutter, Gaussian Basis Sets for Accurate Calculations on Molecular Systems in Gas and Condensed Phases. *J. Chem. Phys.* 127, 114105 (1-9) (2007).
- [9] J. Hutter, M. Iannuzzi, F. Schiffmann, J. VandeVondele, cp2k: Atomistic Simulations of Condensed Matter Systems. *WIREs Comput. Mol. Sci.* 4, 15-25 (2014).
- [10] C. Baerlocher, L. B. McCusker, *Database of Zeolite Structures*, <http://www.iza-structure.org/databases/>.
- [11] G. J. Martyna, M. L. Klein, M. Tuckerman, Nose-Hoover chains: The Canonical Ensemble Via Continuous Dynamics. *J. Chem. Phys.* 97, 2635-2643 (1992).
- [12] J. P. Perdew, K. Burke, M. Ernzerhof, Generalized Gradient Approximation Made Simple *Phys. Rev. Lett.* 77, 3865-3868 (1996).

[13] S. Grimme, J. Antony, S. Ehrlich, H. Krieg, A Consistent and Accurate *ab initio* Parametrization of Density Functional Dispersion Correction (DFT-D) for the 94 Elements H-Pu. J. Chem. Phys. 132, 154104-154100 (2010).

[14] S. Goedecker, M. Teter, J. Hutter, Separable Dual-Space Gaussian Seudopotentials. Phys. Rev. B. 54, 1703-1710 (1996).